Probing Dipole and Quadrupole Resonance Mode in Non-plasmonic Nanowire using Raman Spectroscopy

Sreyan Raha[1], Sreemanta Mitra[1]‡, Prasanna Kumar Mondal[2], Subhajit Biswas[3], Justin D Holmes[3] and Achintya Singha[1]*

[1]Department of Physics, Bose Institute, 93/1 Acharya Prafulla Chandra road, Kolkata 700009, India

[2]Department of Physics, Surendranath College, Kolkata 700009, India

[3]Materials Chemistry and Analysis Group, School of Chemistry,University College Cork, Cork T12 YN 60, Ireland

E-mail: achintya@jcbose.ac.in

Abstract. Electric field enhancement in semiconductor nanostructures offers a possibility to find an alternative to the metallic particles which is well known for tuning the light-matter interaction due to its strong polarizability and size-dependent surface plasmon resonance energy. Raman spectroscopy is a powerful technique to monitor the electric field as its scattering depends on the electromagnetic eigenmode of the particle. Here, we observe enhanced polarized Raman scattering from germanium nanowires of different diameters. The incident electromagnetic radiation creates a distribution of the internal electric field inside the naowires which can be enhanced by manipulating the nanowire diameter, the incident electric field and its polarization. Our estimation of the enhancement factor, including its dependence on nanowire diameter, agrees well with the Mie theory for an infinite cylinder. Furthermore, depending on diameter and wavelength of incident radiation, polarized Raman study shows dipolar (antenna effect) and quadrupolar resonances, which has never been observed in germanium nanowire. We attempt to understand this polarized Raman behavior using COMSOL Multiphysics simulation, which suggests that the pattern observed is due to photon confinement within the nanowires. Thus, the light scattering direction can be toggled by tuning the polarization of incident excitation and diameter of non plasmonic nanowire.

‡ Present address: Department of Physics, Indian Institute of Science, Bangalore 560012, India.

1. Introduction

Scientists devote extensive effort to study light-matter interaction at the nanoscale as nanostructure systems offer its dimension dependent coupling with the electromagnetic field.[1, 2] In recent years rapid development in technologies triggered nanowires' immense applicability in photovoltaic, photo sensor and solar cell[3, 4, 5, 6, 7, 8] etc. This application requires efficient coupling of nanostructures with electromagnetic (EM) field[9, 10, 11]. One of the most familiar ways to increase efficiency of coupling is to decorate the parent material with metal particles. The strongly localized EM field at the vicinity of the metal nanoparticles enriches the hybrid materials for application as Surface Enhanced Raman Scattering (SERS) substrates for ultra sensitive detection of biomolecules.[12, 13, 14, 15, 16, 17]. The EM energy stored inside a dielectric cylinder, which is irradiated by an EM plane wave, was evaluated analytically by Ruppin in 1998 [18], who demonstrated that the stored energy exhibits resonant enhancement near the locations of the cylinder extinction resonances. In semiconductor and insulating materials, realization of such enhancement of an EM field is significant for potential applications in photonic technology and semiconductor electronics. Recently, the enhancement of the EM radiation in Si, InAs has been reported [19, 20]. Among the different materials available in silicon photonics, germanium(Ge) plays a key role in setting up important functionalities required for a photonic integrated platform [21]. The small energy difference between the direct and the indirect band gap of Ge also makes it an ideal material to develop electro-absorption modulator (EAM)[22, 23]. It is reported that the direct bandgap Ge can be obtained by applying tensile strain [24, 25]. Recent report on the realization of the direct band gap Ge nanowire due to Sn doping opens up unlimited possibilities in group IV photonics, nanoelectronics and optoelectronics.[26]. Therefore, the study of EM field enhancement in Ge nanowires (NWs) is highly desirable. Raman scattering is a powerful and sensitive method to probe the internal field enhancement as it exhibits a strong resonant effect when the energy of the incident radiation is comparable with that of EM eigenmode of a dielectric particle.

We report intrinsic internal field induced Raman enhancement for TM (Transverse Magnetic) and TE (Transverse Electric) waves from isolated Ge NWs with certain combinations of NW diameters and incident excitations. Assuming a NW as an infinite cylinder, the calculated field enhancement factors as a function of wavelength of optical excitation and radius of a NW are consistent with the Raman scattering data. This study reveals that for resonant field enhancement there is an interplay between the diameter of a NW and the incident excitation which we tried to understand through the resonant behavior between the incident EM field and the geometry of dielectric particle. Our study extends to the polarization dependent Raman response of the NWs of three different diameters, which shows that the antenna effect and multipolar behavior of polarized Raman response are strongly dependent on the wavelength of incident excitation and NW diameter. This phenomenon has been explained by considering photon confinement. This observed diameter and polarization dependent behavior of localized EM field in semiconducting materials under EM radiation, particularly for Ge having a low band gap energy and high hole mobility, may have important implications for future optoelectronics applications.[27, 28, 29, 30, 31, 32]

2. Experiment

Ge nanowire growth was carried out in a toluene medium using a liquid-injection chemical vapor deposition (LICVD) technique[33]. Au nanopar-

ticles, with average diameter of 5 nm, were spin-coated onto a Si (001) substrate and loaded into a stainless steel micro reactor cell, connected to metal tubing. A Solution of diphenylgermane (DPG) in anhydrous toluene (concentration: 10 μmol ml^{-1}) was injected into the metal reaction cell using a Hamilton sample-lock syringe and syringe pump at a rate of 0.025 ml min^{-1}. A H_2/Ar flow rate of 0.5 ml min^{-1} was maintained during the entire growth period. The NW were grown at 440^{o}C. A typical NW growth time was 2 hr. Bottom-up grown Ge NWs were imaged on an FEI Helios NanoLab 600i scanning electron microscope (SEM). High resolution Scanning Transmission Electron Microscope (STEM) imaging was undertaken using a Nion UltraSTEM100 microscope, operated at 100 kV. Raman measurements were performed on a LABRAM HR spectrometer equipped with 1800 lines/mm grating and a peltier cooled CCD detector for collection of the data. A He-Ne laser of wavelength 633 nm and an air-cooled Argon-ion laser (Ar^+) of wavelength 488 nm were used as excitation light sources, and a 100X objective with numerical aperture (NA) of 0.9 was used to focus the laser on the sample and to collect the scattered light from the sample. Ge NWs were transferred onto InAs substrates and Raman data were collected from the NWs at a backscattering geometry. Throughout the measurements, laser power was kept constant.

3. Results and Discussions

Figure 1(a) shows the successful growth of Au catalyzed Ge NWs after a 2 hr time period, as determined by SEM and STEM. The minimal amount of particulate deposits, as a by product, on the NW surfaces and within the samples in general verifies the controlled growth of the NWs. The NWs grown were straight without any observed kinks, bends or curling. The lengths of the NWs were in the order of several micrometers (>5 μm), whereas their diameters vary between 50-200 nm. The large variation in the nanowire diameter is due to the use of very small (5 nm) Au nanoparticle seed as growth promoter, which forms eutectic liquid at growth temperature and aggregates during nanowire growth, resulting large diameter variation. The presence of partially spherical seeds at the tips of the NWs, as seen in the high resolution SEM image in the inset of Figure 1(a), confirms the participation of catalytic vapor liquid solid (VLS) NW growth [33]. Figure 1(b) shows a high resolution STEM image of a representative NW from the sample using the high angle annular diffraction (HAADF) mode. The image was recorded with <110> zone axis alignment. Generally, the crystal structure of the Ge NWs exhibit a bulk diamond cubic crystal structure with a 3C lattice arrangement without any stacking faults and twin boundaries, with <111> being the dominant growth direction as also confirmed by the Fast Fourier transform (FFT) analysis of the image [inset of Figure 1(b)].

Typical Raman measurement geometry for the transferred Ge NWs is presented in Figure 2.(a). For polarization dependent measurements, a half wave plate was used as a polarization rotator and a vertical analyzer was used at the collection side. Raman measurement geometry for TM and TE waves are also presented in Figure 2(a). Figure 2(b) shows Raman spectra for TM and TE waves from bulk Ge and Ge NWs of various diameters (d): 76 nm (Ge 1), 95 nm (Ge 2), 110 nm (Ge 3), 116 nm (Ge 4) 146 nm (Ge 5), 170 nm (Ge 6) excited by 633 nm laser. The same data using 488 nm laser are presented in Figure S1(Supplementary Materials). The peak due to the triply degenerate E_{2g} mode of Ge appears around 303 cm^{-1} in a bulk sample. As the diameter decreases, the Raman peak positions for both TM and TE waves shifted towards lower frequency, which is due to the confinement of

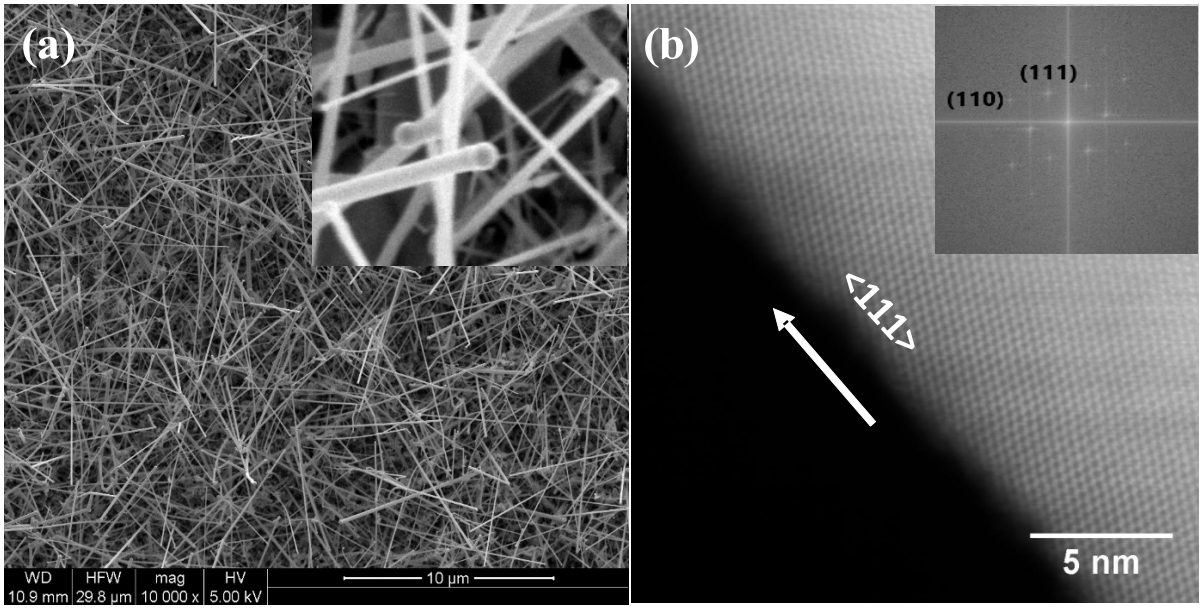

Figure 1. (a) SEM images of Au catalyzed Ge NWs showing NW morphology.Inset shows the high resolution SEM image. (b) Lattice-resolved STEM HAADF image recorded from a representative Ge NW shows its single crystalline nature with a diamond cubic crystal structure. FFT pattern in the inset confirms the crystallinity and growth orientation of the Ge NW.

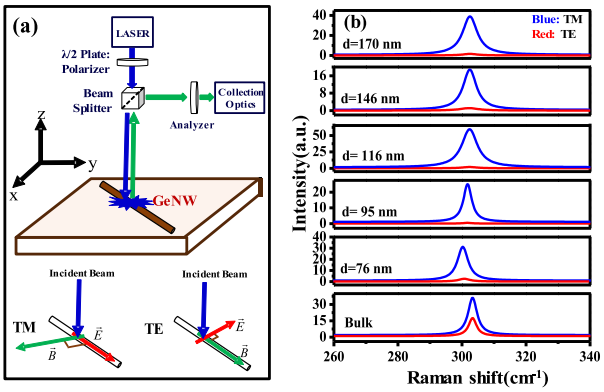

Figure 2. (a) Illustration of the Raman measurement geometry of a Ge NW transferred on a InAs substrate for TM and TE waves. (b) Raman spectra using a 633 nm laser for TM (blue) and TE (red) waves from various NWs, whose diameter, d is indicated in the figure.

phonons at low dimensions[34]. It is worth noting that all data were recorded at very low laser power [laser power∼0.02 mW], which excludes the possibility of laser induced heating effects. To obtain an insight into the intrinsic enhancement of Raman signal from the NWs compared to bulk Ge, we define the Enhancement Factor(EF) as

$$S = \frac{I_{NW}/V_{NW}}{I_{Bulk}/V_{Bulk}}$$

where, I_{NW} is the Raman intensity from the centre of the NW, V_{NW} is the volume of the NW illuminated by the laser, I_{Bulk} is the Raman intensity from bulk Ge and V_{Bulk} is the volume of bulk Ge illuminated by the laser.

The estimated Raman EF for TM and TE waves were calculated for both the 633 nm and 488 nm lasers and plotted as a function of NW radius (R), as shown in Figures 3(a) and (b). The enhancement of the TM waves was higher than for the TE waves. In order to support our experimental data we performed a simulation based upon Mie scattering theory for infinite cylinder. We consider an infinite cylinder and solve Maxwell's equations using boundary conditions of cylindrical azimuthal symmetry[See Supplementary Materials]. The results obtained are shown by red lines (633 nm) and blue lines (488 nm) for TM and

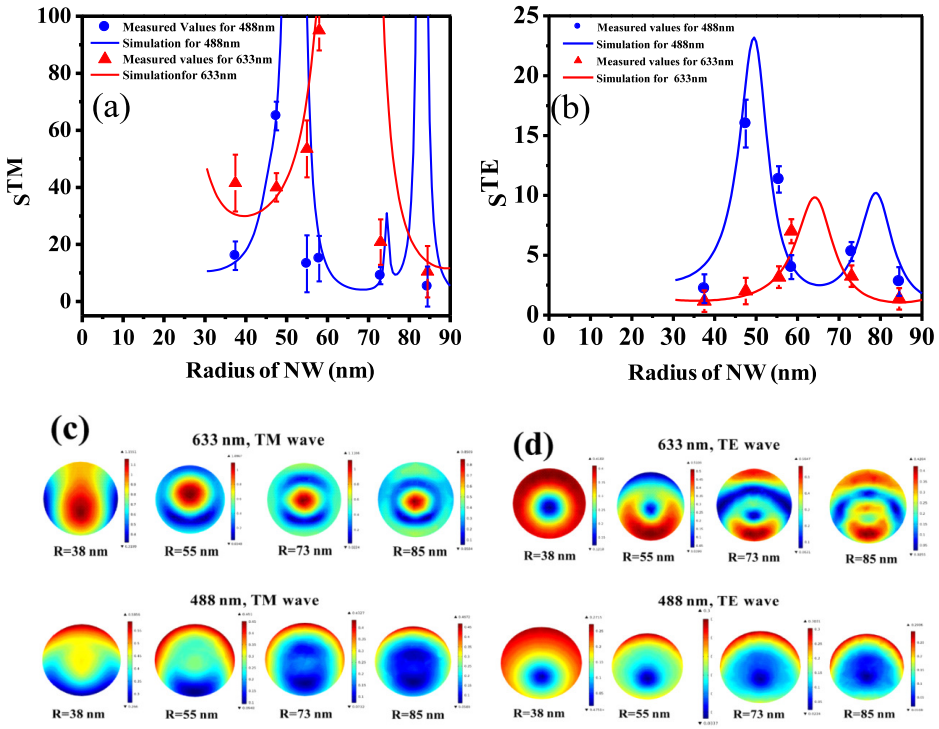

Figure 3. (a) Enhancement factor of TM waves for incident excitations of 488 nm and 633 nm (b) Enhancement factor for TE waves for incident excitations of 488 nm, 633 nm, where continuous curves (blue: 488 nm, red: 633 nm) are theoretical curves according to Mie Theory for an infinite cylinder and descrete points are experimental values for various radii.(c), (d) Internal electric field spatial distribution for various radii ranging from R=38 nm to R=85 nm while incident excitation is 633 nm and 488 nm (as labelled in the figure) for TM and TE waves respectively.

TE waves as shown in Figure 3.(a) and 3.(b) respectively. At both laser wavelengths, the calculated enhancement for TM and TE waves followed the experimental data. It is interesting to note that the resonant enhancement in both TM and TE waves strongly depends on the wavelength and polarization state of the incident excitation, along with the size of the nanoantenna. We attribute this to the resonant nature between cross-section of a NW and the incident excitation. [19]

The distribution of the internal electric field over radial crosssection of the NW, can be understood from the Electromagnetic Waves, Frequency Domain Interface (EWFDI) simulation in the COMSOL. We consider cylindrical Ge nanoantenna with different diameters for the simulation. The electrodynamics is governed by the semi-classical Maxwell equation, given by

$$\vec{\nabla} \times \mu_r^{-1}(\vec{\nabla} \times \vec{E}) - k_0^2(\varepsilon_r - \frac{j\sigma}{\omega\varepsilon_0})\vec{E} = 0$$

μ_r is the relative permeability of the medium, k_0 is wave vector of light in free space, ε_r is the relative permitivity of the medium, ε_o is permitivity in free space, σ is electrical conductivity.

Figure 3(c) shows the color-coded amplitude maps of calculated electric field within the radial cross-section of several Ge NW radii between R=38 nm and R=85 nm when irradiated by 633 nm and 488 nm lasers in the TM configuration. The amplitude color scale is different for different nanoantenna radii to allow the pattern to be more easily observed. The figure shows how the internal electric field evolved as radius of

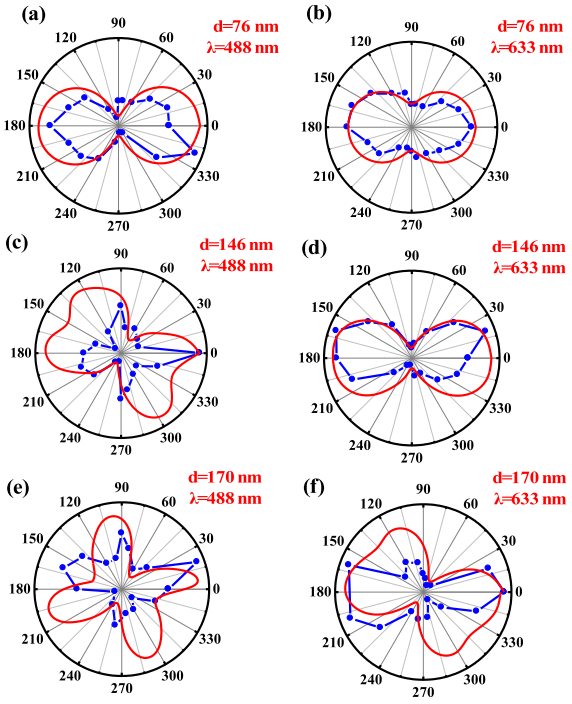

Figure 4. (a),(c),(e) Polarized Raman response from individual NWs excited at a wavelength of 488 nm, with diameters of 76, 146 and 170 nm respectively. (b), (d), (f) Polarized Raman response from individual NWs excited at a wavelength of 633 nm, for diameters of 76, 146 and 170 nm respectively. Blue points and curves show the experimentally observed patterns while the red curves show the simulated data for all figures.

a NW increases. For the 633 nm laser, the maximum localized electric field appears around the centre of the radial cross-section of the NW and spatial extension of the maxima decreases with increasing NW diameter. For the 488 nm wavelength we also observed the maximum localized electric field around the center of the radial cross-section and the maxima shifts away from the centre as the NW radius increases. For TE waves, the minimum amplitude of the electric field appeared at the centre for both excitations (488 nm and 633 nm)[Figure 3 (d)]. For the 633 nm laser, as radius increases, the electric field set up in the NWs forms complex patterns depending upon incident excitation and after a critical diameter, it forms higher order resonance peaks. The complex pattern of electric field inside nanoantenna may be due to the leaky mode resonance (LMR)[35, 36, 37].

To understand the electric field profile inside the nanoantennas, we performed a polarization dependent Raman study as Raman mode intensity directly relates to the induced electric field [19, 20]. Systematic polarization dependent Raman response of the E_{2g} mode are plotted in Figure 4 for Ge1, Ge5 and Ge6. To check the repeatability, we have measured five-time and the plots in Figure 4 are the average of five-time measured data. We observe an dipole (antenna) effect for Ge1 (76 nm) for both the lasers. A signature of quadrupole appeared at Ge 5 (146 nm) for the 488 nm laser whereas, for the 633 nm laser quadrupole was only observed for Ge 6 (170 nm). All theoretical calculations based on symmetry of phonon wave function predict that the cross-section of Raman scattering is minimized for cross polarized (TE waves) and maximum for parallel polarization (TM waves), giving antenna effect[38, 39, 40, 1, 41]. It is due to the fact that the Raman tensor involved in the calculation contains a dipole term. But, here we observe antenna effect as well as quadrupolar pattern depending on the NW diameter and the incident excitation. So, our data may have no correlation with the symmetry of the wave function of the phonon[42]. The behavior may be associated with the classical scattering of electromagnetic waves from a cylindrical dielectric system. To confirm this, we have calculated the intensity of the electric field as a function of polarization in Ge1, Ge5 and Ge6 NWs using COMSOL. We compare the polarized Raman data (Blue curve in Figure 4) with the calculated (Red curve in Figure 4) polarization dependent field intensity. The simulation deviates from the experimental result. A possible explanation for the deviation is that the complex diameter dependent transmission of the Raman scattered light across the nanowire-

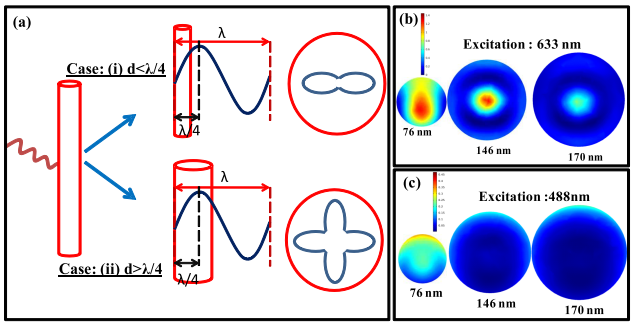

Figure 5. (a) Schematic diagram to explain the diameter and wavelength dependent polarized Raman spectroscopic behavior. (b), (c) Intensity contour plot of the radial cross-section where ratio of sizes matches with actual radial size of the NWs for TM waves when excited at 633 nm and 488 nm respectively.

air interface [43, 44, 45]. Moreover, surface facets and the exact cross-sectional shape of the nanowire, which could modify the Raman scattering intensity, were not considered in our simulation. Though there is a mismatch between the measured and the simulation data, however, experimental data presented in Figure 4 c and e show emergence of the quadrupolar pattern from the dipolar pattern as observed previously in plasmonic nanostructures [46]. Thus the experimental results qualitatively agree to the simulation.

As the diameter changes, the polarized Raman response of NWs is modified. The correlation between diameter of nanowire and incident excitation can be understood through the mechanism presented in Figure 5.(a). When light of a particular wavelength (λ) is incident on a material, the medium behaves as continuous or discontinuous for the λ depending on the relation between λ and size of the material. Here, it is seen that, when the NW diameter is much lower than λ, then the incident excitation is unable to resolve the internal structure of the NW. Incident excitation seems to look into the NW as a whole [See Figure 5.(a)]. Thus the geometry of the NW behaves as continuous with respect to the incident excitation and plays an important role in controlling the optical response. For such cases ($d < \lambda/4$), we observe antenna effect, i.e. in case of the nanowire with lowest diameter (76 nm). On the other hand, when d is large($d > \lambda/4$), then the medium behaves as discontinuous with respect to the incident λ and the geometry does not play any role in the optical response. For such cases, quadrupole behavior is observed [see Figure 5.(a)] [42]. Figure 5.(b) and (c) show the contour plot of the calculated intensity of radial cross-section for TM waves at excitation wavelengths of 633 nm and 488 nm for nanoantennas of different diameters as indicated in the figures. In both cases, the cross-sections are comparable with the cross-section of the corresponding NW. For d=76 nm, at both excitation wavelengths of 488 nm and 633 nm, photons are confined as indicated by the central bright spot in the cross-section of the TM waves and in both cases, we observe an antenna effect [Fig 4(a), (b)]. But with the increasing NW diameter, photon confinement gets weaker. Strong photon confinement exists upto d=146 nm at 633 nm, whereas at 488 nm, the confinement exists only at d=76 nm [See Figure 5.(b), (c)]. The quadrupole behavior appears at d=146 nm for 488 nm laser [Figure 4.(c)] but at d=170 nm for 633 nm laser[Figure 4.(f)], which correlates nicely with the photon confinement showed in figure 5.(b), (c). The whole scenario is summarized in the Table.

4. Conclusions

In summary, we observe intrinsic enhancement of the EM field in Ge NWs. Its dependence on incident excitation energy and polarization of incident excitation were investigated. The pattern of evolution of the enhancement factor with radius of NW has also been simulated on basis of Mie theory for an infinite cylinder, which is in agreement with our experimental

Diameter of NW(d)	Polarization dep. Raman response using		Remarks [PC stands for Photon Confinement]
	488 nm	633 nm	
76 nm	Dipole	Dipole	PC occurs for both the lasers.
146 nm	Quadrupole	Dipole	PC occurs only for 633 nm.
170 nm	Quadrupole	Quadrupole	No PC for both the lasers

Raman data. Simulation shows how the electric field pattern inside the NW changes with their radius for both TM and TE waves with different incident excitation. To get more insight, the polarized Raman response over a 360^o angle dependence was studied for NWs with three different diameters. Our study revealed that the polarized Raman response shows dipole or quadrupole depending on NW diameter and the wavelength of incident excitation. The Simulated polarization dependent electric field intensity was qualitatively in agreement with the experimentally observed Raman intensity pattern. Our simulation further correlates this polarized Raman behavior with photon confinement. Thus Ge nanoantenna couples enhanced optical field with propagating radiation. Therefore, our result may be useful to understand dimension and geometry dependent optical response from non plasmonic nanostructures and also for any Ge based future opto-electronic devices, where efficient light matter interaction is desired.

Acknowledgement

Authors acknowledge Kabita Kundalia, Bose Institute, Kolkata, for useful discussions regarding Mathematica Code. JDH acknowledges financial support from Science Foundation Ireland (Grant: 14/IA/2513).

References

[1] Mühlschlegel, P. and Eisler, H.-J. and MartinO., J. F. and Hecht, B. and Pohl, D. W., 2005 *Science* **308**, 5728.

[2] Kuznetsov, Arseniy I. and Miroshnichenko, Andrey E. and Brongersma, Mark L. and Kivshar, Yuri S. and Luk'syanchuk, Boris 2016 *Science* **354**, aag2472.

[3] C. M. Lieber 2011 *MRS Bulletin* **36**, 1052-1063.

[4] Brubaker, Matt D. and Blanchard, Paul T. and Schlager, John B. and Sanders, Aric W. and Roshko, Alexana and Duff, Shannon M. and Gray, Jason M. and Bright, Victor M. and Sanford, Norman A. and Bertness, Kris A. 2013 *Nano Lett.* **13**, 374-377.

[5] Richard Soref 2010 *Nat. Photonics* **4**, 495- 497.

[6] Bjork, M. T. and Ohlsson, B. J. and Sass, T. and Persson, A. I. and Thelander, C. and Magnusson, M. H. and Deppert, K. and Wallenberg, L. R. and Samuelson, L. 2002 *Appl. Phys. Lett.* **81**, 4458-4460.

[7] Funes-Hernando, D. and Pelaez-Fernandez, M. and Winterauer, D. and Mevellec, J.-Y. and Arenal, R. and Batten, T. and Humberta, B. and Duvail, J. L. 2018 *Nanoscale* **10**, 6437-6444.

[8] Liu, Fei and Mo, F. Y. and Jin, S. Y. and Li , L. and Chen, Z. S. and Sun, R. and Chen, J. and Deng, S. Z. and Xu, N. S. 2011 *Nanoscale* **3**, 1850-1854.

[9] Alivisatos, A. P. 1996 *Science* **271**, 933-937.

[10] Vahala, Kerry J. 2003 *Nature* **424**, 839–846.

[11] Novotny, Lukas and Hulst, Niek van 2011 *Nat. Photonics* **90**, 83-90.

[12] Shuming, Nie and Steven, R. Emory 1997 *Science* **275**, 1102-1106.

[13] Atakaramians, Shaghik and Miroshnichenko, Andrey E. and Shadrivov, Ilya V. and Mirzaei, Ali and Monro, Tanya M. and Kivshar, Yuri S. and V., Shahraam Afshar 2016 *ACS Photonics* **3**, 972-978.

[14] Peter, Manuel and Hildebrandt, Andre and Schlickriede, Christian and Gharib, Kimia and Zentgraf, Thomas and Forstner, Jens and Linden, Stefan 2017 *Nano Lett.* **17**, 4178-4183.

[15] Kneipp, Kartin and Wang, Yang and Kneipp, Harald and Perelman, Lev T. and Itzkan Irving and Dasari Ramachandra R. and Feld, Michael S. 1997 *Phys.*

Rev. Lett. **78**, 1667-1670.

[16] Kneipp, K. and Kneipp, H. and Deinum, G. and Itzkan, I. and Dasari, R. R. and Feld, M. S 1998 *Applied Spectroscopy* **52**, 175-178.

[17] Liang, H. and Li, Z. and Wang, W. and Wu, Y. and Xu, H. 2009 *Nat. Advanced Materials* **21**, 4614-4618.

[18] Ruppin, R. 1998 *Journal of the Optical Society of America A* **15**, 1891-1895.

[19] Cao, Linyou and Nabet, Bahram and Spanier, Jonathan E. 2006 *Phys. Rev. Lett.* **96**, 157402.

[20] Panda, Jaya Kumar and Roy, Anushree and Singha, Achintya and Gemmi, Mauro and Ercolani, Daniele and Pellegrini, Vittorio and Sorba Lucia 2013 *Solid State Commun.* **160**, 26-31.

[21] Morini,Delphine Marris and Vakarina, Vladyslav and Ramireza,Joan Manel and Liua, Qiankun and Ballabio,Andrea and Frigerio,Jacopo and Montesinos, Miguel and Alonso-Ramos,Carlos and Roux, Xavier Le and Sernab,Samuel and Benedikovic, Daniel and Chrastina,Daniel and Vivien, Laurent and Isella, Giovanni 2018 *Nanophotonics* **7**, 1-13.

[22] Feng, Ning-Ning and Feng, Dazeng and Liao, Shirong and Wang, Xin and Dong, Po and Liang, Hong and Kung, Cheng-Chih and Qian, Wei and Fong, Joan and Shafiiha, Roshanak and Luo, Ying and Cunningham, Jack and Krishnamoorthy, Ashok V. and Asghari, Mehdi 2011 *Optics Express* **19**, 7062-7067.

[23] Greytak, Andrew B. and Barrelet, Carl J. and Li, Yat and Lieber, Charles M. 2005 *Appl Phys Lett* **87**, 151103.

[24] Soref, Richard A. and Friedman, Lionel 1993 *MRS Superlattices and Microstructures* **14**, 189-193.

[25] Lim, Peng Huei and Park, Sungbong and Ishikawa, Yasuhiko and Wada, Kazumi 2009 *Optics Express* **17**, 16358-16365.

[26] Biswas, S. and Doherty, J. and Saladukha, D. and Ramasse, Q. and Majumdar, D. and Upmanyu, M. and Singha, A. and Ochalski, T. and Morris, M. A. and Holmes J. D. 2016*Nat. Commun.* **7**, 11405.

[27] Kelzenberg, Michael D. and Turner-Evans, Daniel B. and Kayes, Brendan M. and Filler, Michael A. and Putnam, Morgan C. and Lewis, Nathan S. and Atwater, Harry A. 2007 *Nano Lett* **8**, 710-714.

[28] Tian, Bozhi and Zheng, Xiaolin and Kempa, Thomas J. and Fang, Ying and Yu, Nanfang and Yu, Guihua and Huang, Jinlin and Lieber, Charles M. 2007 *Nature* **449**, 885–889.

[29] Garnett, Erik C. and Yang, Peidong 2008 *J. Am. Chem. Soc.* **130**, 9224–9225.

[30] Chu, X.-L. and Brenner, T. J. K. and Chen, X.-W. and Ghosh, Y. and Hollingsworth, J. A. and Sandoghdar, V. and Götzinger, S. 2014 *J. Optica* **1**, 203-208.

[31] Joycea, Hannah J. and Gao, Qiang and Tan, H.Hoe and Jagadish, C. and Kim, Yong and Zou, Jin and Smith, Leigh M. and Jackson, Howard E. and Yarrison-Rice, Jan M. and Parkinson, Patrick and Johnston, Michael B. 2011 *Progress in Quantum Electronics* **35**,23-75.

[32] Wang, Zhihuan and Nabet, Bahram 2015 *Nanophotonics* **4**, 491–502.

[33] Biswas, Subhajit and Regan, Colm O' and Petkov, Nikolay and Morris, Michael A. and Holmes, Justin D. 2012 *Nano Lett.* **12**, 5654-5663.

[34] Mak, Kin Fai and Lee, Changgu and Hone, James and Shan, Jie and Heinz, Tony F. 1986 *Solid State Commun.* **58**, 739-741.

[35] Cao, Linyou and White, Justin S. and Park, Joon-Shik and Schuller, Jon A. and Clemens, Bruce M. and Brongersma, Mark L. 2009 *Nature Materials* **8**, 643-647.

[36] Cao, Linyou and Fan, Pengyu and Vasudev, Alok P. and White, Justin S. and Yu, Zongfu and Cai, Wenshan and Schuller, Jon A. and Fan, Shanhui and Brongersma, Mark L. 2010 *Nano Lett.* **10**, 439-445.

[37] Barnard, Edward S. and Pala, Ragip A. and Brongersma, Mark L. 2011 *Nature Nanotechnology* **6**, 588-593.

[38] Duesberg, G. S. and Loa, I. and Burghard, M. and Syassen, K. and Roth, S. 2000 *Phys. Rev. Lett.* **85**, 5436-5439.

[39] Jorio, A. and Souza, A.G. and Brar, V.W. and Swan, A.K. and Unlu, M.S. and Goldberg, B.B. and Righi, A. and Hafner, J.H. and Lieber, C.M. and Saito, R. and Dresselhaus, G. and Dresselhaus, M.S. 2002 *Phys. Rev. B* **65**, 155412.

[40] Saito, R. and Takeya T. and Kimura, T. and Dresselhaus, G. and Dresselhaus, M. S. 1998 *Phys. Rev. B* **57**, 4145.

[41] Rafailov, P. M. and Thomsen, C. and Gartsman, K. and Kaplan-Ashiri, I. and Tenne R. 2005 *Phys. Rev. B* **72**, 1607-1609.

[42] Xiong, Q. and Chen, G. and Gutierrez, H.R. and Eklund, P.C. 2006 *Applied Physics A* **85**, 299–305.

[43] Lopez, F. J. and Hyun, J. K. and Givan, U. and Kim, I. S. and. Holsteen, A. L. and Lauhon, L. J. 2012 *Nano Lett.* **12**, 22662271.

[44] Tarun, A. and Hayazawa, N. and Ishitobi, H. and Kawata, S. and Reiche, M. and Moutanabbir, O. 2011 *Nano Lett.* **11**, 47804788.

[45] Chew, H. and Cooke, D. D and Kerker, M. 1980 *Appl.*

Opt. **19**, 4452.

[46] Fernandez, Jessica Rodrıguez and Juste, Jorge Perez and Abajo, F. Javier Garcıa de and Marzan, Luis M. Liz. 2006 *Langmuir* **22**, 7007-7010.